

# 1 Numerical study on the heat transfer performance of mine ice-storage 2 cooling device

3

4 Weishuang Guo<sup>a</sup>, Zujing Zhang<sup>a,b\*</sup>, Xing Liang<sup>c</sup>, Hongwei Wu<sup>d</sup>, Liang Ge<sup>b</sup>, Ruiyong Mao<sup>a\*\*</sup>5 <sup>a</sup> College of Civil Engineering, Guizhou Provincial Key Laboratory of Rock and Soil Mechanics and Engineering  
6 Safety, Guizhou University, Guiyang, 550025, China.7 <sup>b</sup> State Key Laboratory of Coal Mine Disaster Prevention and Control, Chongqing Research Institute of China  
8 coal Technology and Engineering Group Co. Ltd., Chongqing, 400037, China.9 <sup>c</sup> School of Computer Science and Mathematics, Kingston University London, KT1 2EE, United Kingdom10 <sup>d</sup> School of Physic, Engineering and computer science, University of Hertfordshire, Hatfield, AL10 9AB, United  
11 Kingdom.12 \*Corresponding author: [tel: +86 185 2391 9513](tel:+8618523919513) email: [zjzhang3@gzu.edu.cn](mailto:zjzhang3@gzu.edu.cn).13 \*\*Corresponding author: [tel: +86 139 8505 6628](tel:+8613985056628) email: [rymao@gzu.edu.cn](mailto:rymao@gzu.edu.cn).

14

15 **Abstract:** The thermal performance of the ice-storage cooling device used in the underground  
16 mine refuge chamber is poor, which causes a waste of energy. Therefore, it is necessary to improve  
17 the heat transfer performance of ice latent heat storage devices. In the current work, the effects of  
18 fin height, fin thickness and number of fins on the heat transfer performance of the ice based latent  
19 heat energy storage device were numerically analyzed. The results show that: (i) when the number  
20 of fins is 8, the heat exchange characteristics of the ice-storage device reaches the best performance;  
21 (ii) increasing the number of fins and the height of the fins can increase the heat exchange area and  
22 improve the heat exchange performance; (iii) compared with the ice-storage device without fins, the  
23 cooling efficiency of the ice-storage device increased by 34.12% and the melting rate increased by  
24 9.3% after the addition of fins. The addition of fins can improve the heat exchange efficiency of the  
25 ice-storage device, while promote the application of phase change energy storage technology in  
26 underground mine refuge chambers.

27 **Keywords:** Mine refuge chamber, CFD, Ice based latent heat energy storage, Heat transfer, Fins.

28

<i>Nomenclature</i>		<i>Subscripts</i>	
$C_m$	Mushy zone constant	$h_r$	Reference surface enthalpy, kJ/kg
$C_1, C_2, C_3$	Model parameters	$h_{ss}$	Material sensible enthalpy, kJ/kg
$E$	Enthalpy of the phase transition, kJ/kg	$h_1$	Cold air enthalpy, kJ/kg
$g$	gravity acceleration, $m/s^2$	$h_2$	Hot air enthalpy, kJ/kg
$H$	The height of the fins, mm	$i$	Vector direction
$N$	The number of the fins	$j$	Vector direction
$p$	Pressure, Pa	$T_r$	Reference surface temperature, °C
$Q$	Ice storage capacity, %	$T_{so}$	Water solidification temperature, °C
$R_0$	The diameter of the ice bucket, mm	$T_{li}$	Water melting temperature, °C
$R_1$	The inner diameter of the heat exchanger tube, mm		
$R_2$	The outer diameter of the heat exchanger tube, mm		
$T$	The thickness of the fins, mm		
<i>Greek symbols</i>		<i>Acronyms</i>	
$\alpha$	Coefficient of thermal expansion, 1/K	AOT	Average temperature
$\tau$	Time, h	FH	Fin height
$\omega$	Constant, 0.0001	FN	Fin number
$\gamma$	Liquid volume fraction	FT	Fin thickness
$\varepsilon$	Turbulent energy dissipation, $J/(kg \cdot s)$	IAT	Inlet air temperature
$\kappa$	Turbulent kinetic energy, (J/kg)	IAV	Inlet air velocity
$\lambda$	Thermal conductivity, $W/m \cdot K$	IMR	Ice melting rate
$\mu$	Dynamic viscosity coefficient, $N \cdot s/m^2$	ISCD	Ice-storage cooling device
$\nu$	Motion viscosity coefficient, $m^2/s$	MRC	Mine refuge chamber
$\xi$	Constant, $9.3 \times 10^{-6}$	OAT	Outlet air temperature
$\rho$	Density, $kg/m^3$	SAT	Supply air temperature

# 1. Introduction

Carbon peak and carbon neutrality have become the goals of the development of the energy industry. The effective use of renewable energy is an important way to achieve the "dual carbon" goal<sup>[1-5]</sup>. However, most renewable energy sources, such as geothermal energy, wind energy, solar energy, and tidal energy, have the disadvantages of poor stability and uneven distribution in time and space, renewable energy needs to be stored and converted before it can be reused<sup>[6-10]</sup>. Phase change energy storage technology has been widely used in aviation, ground construction, military industry, and underground space. The research and development of phase change materials and phase change energy storage devices have become the two core elements of phase change energy storage technology<sup>[11-15]</sup>. In the case of determining phase change materials, the structure of the energy storage device is a key factor affecting the heat transfer performance as well as the energy conversion efficiency<sup>[16-20]</sup>.

However, the weak thermal conductivity of most phase change materials leads to low heat transfer efficiency of phase change energy storage devices. In practical engineering, the heat transfer characteristics of phase change energy storage can be improved by increasing the heat transfer coefficient of phase change materials, expanding the heat transfer area, and increasing the heat transfer temperature difference<sup>[21-23]</sup>. Mohsen et al.<sup>[24]</sup> prepared nano-reinforced phase change materials by dispersing nanoparticles in phase change materials, thereby improving the heat transfer coefficient of phase change materials, the effect of an innovative fin structure based on snowflake crystal structure on the heat transfer performance of the energy storage device was analyzed by numerical simulation. Their results showed that the melting rate of the energy storage device increased by 7.8 times after adding fins with snowflake crystal structure, and by 1.2 times after adding nanoparticles with volume fractions of 0.025 and 0.05. Wu et al.<sup>[25]</sup> designed a novel latent heat storage device using spiderweb fins, compared with the traditional plate fins, the complete curing time of the improved energy storage device with spiderweb fins was shortened by 47.9% and the average heat release rate was increased by 1.44 times. Lee et al.<sup>[26]</sup> proposed a new design using layered fins to improve the melting performance of the phase change energy storage device, and their experimental and numerical results showed that the complete melting time of the improved energy storage device was 44.3% shorter than that of the original design. Liu et al.<sup>[27]</sup> proposed a bionic topology to optimise the vertically arranged annular wing to accelerate the heat storage

1 performance, and their numerical results showed that the optimised bionic fin can shorten the  
2 melting time by 45.9% compared with the traditional fin. Lu et al.<sup>[28]</sup> proposed a finned latent heat  
3 transfer device for shell and tube, and established a test rig to analyze the influence of various  
4 factors on the heat transfer performance of the device. They stated that the effective energy release  
5 efficiency of the device is 77% after optimisation. Kurnia et al.<sup>[29]</sup> proposed a rotating phase change  
6 energy storage device, which showed that the rotation did improve the heat transfer performance of  
7 the phase change energy storage device, and the heat transfer efficiency in the energy storage and  
8 energy release processes was increased by 25% and 41%, respectively. Zhang et al.<sup>[30]</sup> introduced an  
9 innovative tree-shaped structure to construct the metal fins of shell-and-tube phase change storage  
10 cells, and investigated and analyzed the effects of length ratio and width index on energy release  
11 performance through numerical simulation. Their results showed that the complete solidification  
12 time of the tree-fin phase change storage unit was reduced by 66.2% and the complete melting time  
13 was reduced by 4.4% compared with the radial fin phase change storage unit. Huang et al.<sup>[31]</sup>  
14 designed an innovative latent heat storage device for palmate fins using biomimetic technology. The  
15 phase transformation behavior and heat transfer modes of biomimetic devices and traditional latent  
16 heat storage devices are studied, and the effects of their arrangement and operating conditions are  
17 revealed. It was concluded that compared with the traditional latent heat storage device, the  
18 performance of the palmate leaf latent heat storage device is significantly improved, and the  
19 complete solidification and melting time are reduced by 21.0% and 38.2%, respectively. The current  
20 research is sufficient to show that the optimisation of the internal structure of the phase change  
21 energy storage device can improve the heat transfer performance of the phase change energy  
22 storage device.

23 When phase change energy storage technology is applied in different research area, it is  
24 necessary to design unique phase change energy storage devices. Aiming at the temperature control  
25 problem of underground high-temperature mine refuge chamber (MRC), Wang et al.<sup>[32]</sup> designed a  
26 forced circulating ice thermal storage system with a single rectangular square tube inside, and their  
27 experimental study showed that the effective cooling time of the system was 64.57 h. Du et al.<sup>[33]</sup>  
28 designed a multi-functional ice storage air conditioning system suitable for 8-person rescue cabins,  
29 and their experimental results showed that the ice storage air conditioning could finally control the  
30 temperature and humidity of the rescue cabin within 31°C and 77%, respectively. Zhang et al.<sup>[34,35]</sup>  
31 designed and fabricated an ice storage and cooling device with a volume of 1 m<sup>3</sup> for the MRC of

1 underground mines, and the heat exchange performance of the device was the best when the number  
2 of heat exchange tubes on the surface was 18, and one ice storage device could meet the cooling  
3 requirements of 8 people in the MRC.

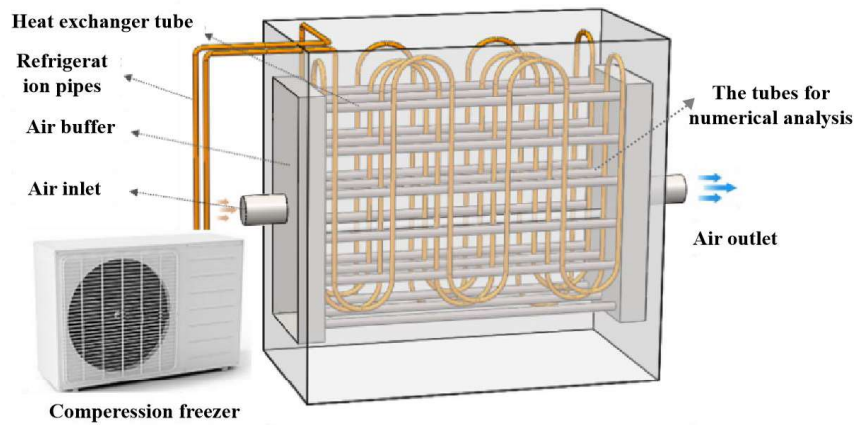
4 Currently, the phase change energy storage technology applied in underground MRCs has  
5 disadvantages in the structural design of energy storage devices, and they are all based on  
6 traditional energy storage devices. Traditional energy storage devices are single round or  
7 rectangular pipes inside, which have much room for improvement in heat transfer efficiency. The  
8 addition of fins to the heat exchanger tubes could improve the heat transfer performance of the  
9 energy storage device, which can reduce the waste of energy during cooling of the underground  
10 MRC. Therefore, in the current work, the internal structure of the mine ice-storage cooling device  
11 (ISCD) will be modified, and fins are added to the periphery of the heat exchange tube to enhance  
12 the heat exchange of the ISCD. According to the current research status, it can be concluded that  
13 with the more complex fin shape and the larger the number of fins, the more obvious the heat  
14 exchange effect of the phase change energy storage device. It is noted that the fins occupy a large  
15 amount of space, resulting in smaller and smaller effective volume. In view of the special  
16 environment of the underground mine refuge chamber, in order to keep the ice storage capacity of  
17 the ice storage device above 83.33%, the rectangular fins are selected in this paper, which can  
18 improve the heat exchange efficiency of the ice storage device and meet the requirements of the ice  
19 storage capacity. In this study, the effects of various impact factors such as fin thickness(FT), fin  
20 height (FH) and fins number(FN) on the heat transfer performance of the ISCD were analyzed  
21 mainly by numerical simulation. The application of the optimised ISCD was discussed and analyzed  
22 in detail, as well as compared with other related studies. The research outcome achieved from the  
23 current work can contribute the theoretical significance of mine ISCD and reduce the energy loss  
24 under limited resources.

## 25 **2. Computational method**

### 26 **2.1 Model description**

27 In this study, the internal structure of the ISCD designed and processed by Zhang et al.<sup>[34]</sup> was  
28 optimised. The reasons for choosing ice in the current study are: the latent heat of the phase change  
29 of ice is large, the raw materials are easy to obtain and the costing is high, as well as the ice will not  
30 bring secondary disasters to the special environment of the mine refuge chamber. Fig. 1 shows an

1 ISCD designed by Zhang et al.<sup>[34]</sup>, there are 18 stainless steel heat exchange tubes with a length of  
2 1.1 m, an inner diameter of 30 mm, and a wall thickness of 2 mm, which are evenly arranged at a  
3 horizontal distance of 0.15 m and a height distance of 0.2 m.



4  
5 **Fig. 1.** Schematic diagram of mine ISCD<sup>[34]</sup>

6 In this study, the heat transfer characteristics and ice melting characteristics of the ISCD were  
7 studied through numerical simulation, and the numerical model was simplified in order to reduce  
8 the time cost in the process of numerical simulation of the structural optimisation of the device.  
9 Taking a single heat exchanger tube as a case study, the heat exchange efficiency of the heat  
10 exchanger tube was enhanced by adding fins, therefore the optimised heat transfer performance of  
11 the whole ice storage and cooling device could be predicted. As shown in Fig. 2, a single heat  
12 exchanger tube in the ISCD is selected and the simplified numerical model is a single tube. The  
13 circular ISCD with a heat influence radius of  $R_0=50$  mm was taken and the inner diameter of the  
14 heat exchanger tube is  $R_1=15$  mm, and the thickness of the tube wall is 2 mm. Fins were arranged  
15 around the heat exchange tube to achieve the effect of enhanced heat exchange. Set the FH to 10  
16 mm, 20 mm, and 30 mm, the FT to 2 mm, 4 mm, and 6 mm, and the FN to 4, 6, and 8. The control  
17 variable method was used to study the effects of the FN, FH and FT on the heat transfer  
18 performance of the ISCD.

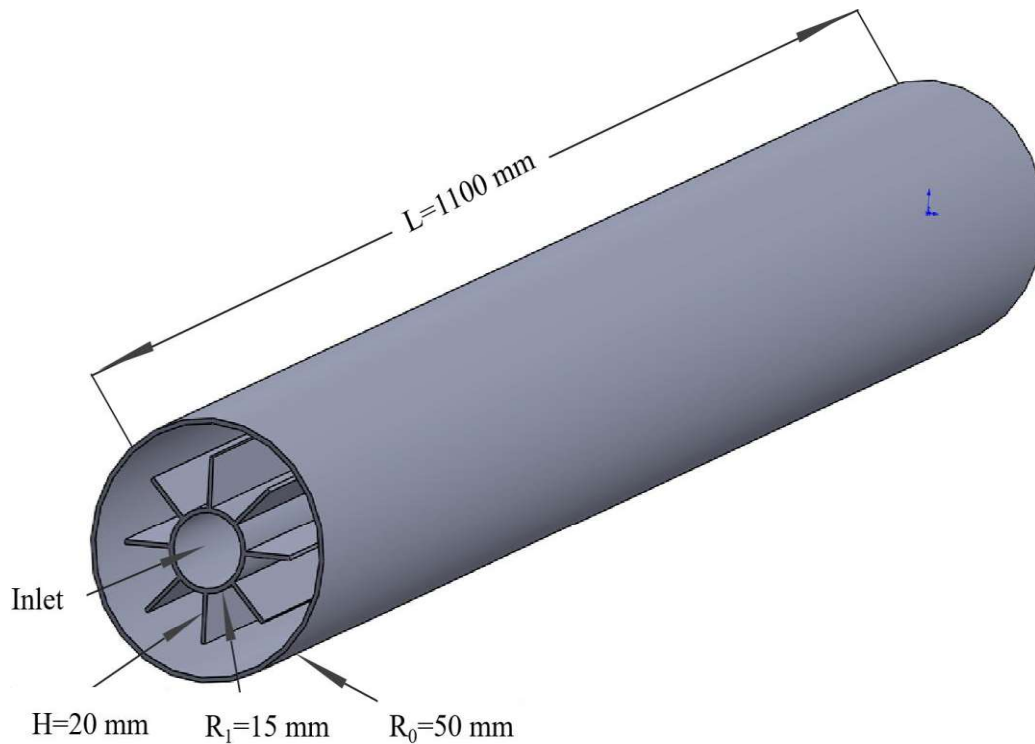


Fig. 2. Simplified schematic diagram of numerical simulation of ISCD

## 2.2 Model construction and grid division

As shown in the Figs. 2 and 3, a simplified numerical model of the ISCD was established using ANSYS ICEM. In the current model, the inner diameter of the heat exchanger tube is 30 mm, the outer diameter is 34 mm, the thickness of the tube wall is 2 mm, and the heat-affected radius of the heat exchanger tube is 50 mm. The non-structural meshing is adopted, and the numerical model has three computational domains, namely the air computational domain, the solid computational domain of the fins and heat exchanger tubes, and the ice-water mixed computational domain. In order to reduce the calculation error of coupled heat transfer at the interface of the two computational domains and better capture the characteristics of the temperature field in the calculation process, the number of meshes on the coupling wall, the wall of the heat exchanger tube bundle, the fin wall, the air inlet and outlet and other surfaces is increased.

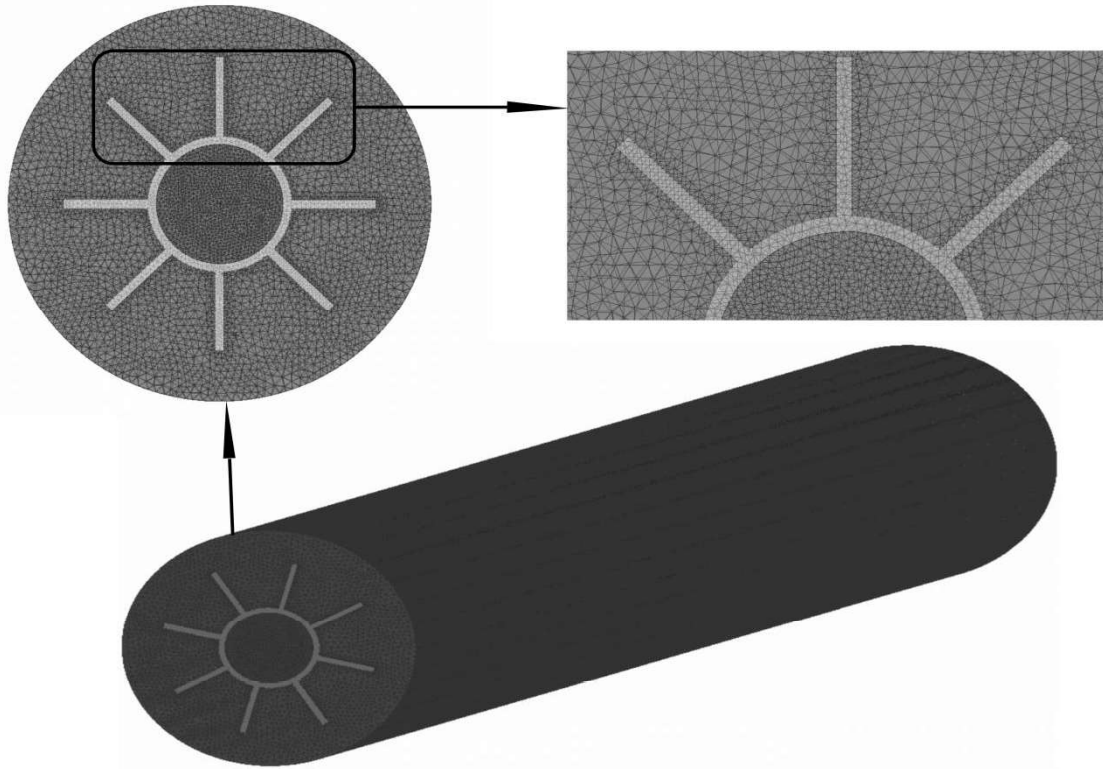


Fig.3. Numerical model meshing diagram

In order to reduce the error caused by the number of meshes to the numerical results, five different meshes (801253, 1256825, 1648926, 2154513, and 2568654) were selected for mesh independence study. During the current simulation work, a computer used is 12-core processor, 64G memory, and 1T solid hard disk. The numerical results with the inlet air temperature (IAT) of 32°C, inlet air velocity (IAV) of 10 m/s and number of heat exchanger tube fins of 8 were selected for the purpose of comparison.

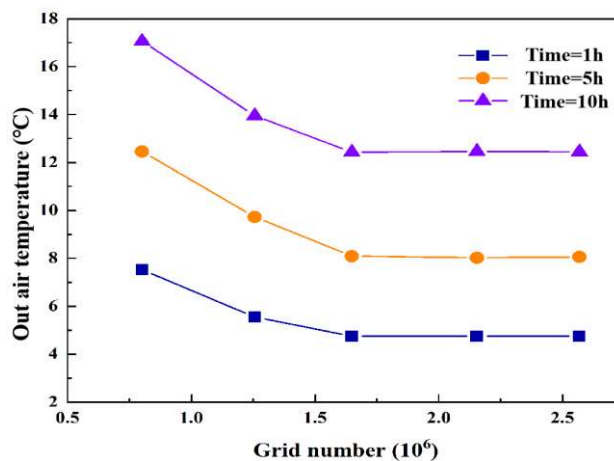


Fig. 4. Grid independence verification

Fig. 4 plots the air temperature change of the air outlet of the ISCD at different times under different grid numbers. It can be observed that the outlet air temperature (OAT) changes significantly when the number of grids is lower than 1648926, after which increasing the number of

1 grids has little effect on the temperature value.

2 [Table 1](#) shows the time cost of calculating the number of meshes

Grid numbers	Heat exchange time	Time step	Calculation time
801253	11 h	2 s	10 h
1256825	11 h	2 s	18.5 h
1648926	11 h	2 s	25 h
2154513	11 h	2 s	36 h
2568654	11 h	2 s	49.5 h

3 It can be seen from [Table 1](#) that when the grid number increases, the time cost of the  
4 calculation increases, and when the number of meshes is small, the calculation accuracy cannot be  
5 satisfied. In the current work, therefore, a grid number of 1648926 with a grid quality of 0.42 is  
6 selected for the following numerical simulation.

### 7 **2.3 Initial conditions and the boundary conditions**

8 The control variable method was used to study the effects of different FH, FT and FN on the  
9 heat transfer performance of the ISCD. The optimised performance of the ISCD should meet the  
10 requirements of 96 h, and the temperature of the MRC should be controlled within 35°C, Zhang et al.  
11 [34] investigated that the cooling effect of the surface ISCD at the IAT of 32°C and the IAV of 10  
12 m/s can meet the temperature control requirements of the MRC. Therefore, all the calculation  
13 models in the present study are set to 32°C and 10 m/s. The numerical working condition design is  
14 shown in [Table 2](#), and the working condition 10 is the model without fins.

15 [Table 2](#). Numerical simulation working condition design table

Case	FH (mm)	FT (mm)	FN (root)
1	10	2	4
2	20	2	4
3	30	2	4
4	20	2	4
5	20	4	4
6	20	6	4
7	20	2	4
8	20	2	6

9	20	2	8
10	0	0	0

The numerical model air inlet is set as the velocity inlet, the outlet is set as the pressure outlet, the interface between the air basin and the ice-water basin of the ISCD model is set as the coupled heat transfer wall, the other walls are set as the adiabatic wall, the heat exchange tube wall and other wall materials are stainless steel, and the initial temperature of each basin is -15°C.

## 2.4 Governing equation

Numerical simulations can effectively solve the problem that the solidification, melting and heat transfer characteristics of ice cannot be visualized during the experiment. The enthalpy porosity method is a reliable method to capture the changes in the ice solidification and thaw interface, and it is widely used to solve the problem of solidification and thawing<sup>[36]</sup>. Yang et al.<sup>[37]</sup> performed a numerical analysis of phase change material (PCM) -air in a circular tube heat exchanger using RNG  $\kappa$ - $\epsilon$  model and the enhanced wall treatment method. Their numerical results showed a good agreement with the experimental data. Therefore, in the present work, the solidification and melting model, the  $\kappa$ -epsilon (RNG) turbulence model and the enhanced wall treatment method are used to simulate the air heat transfer in the tube.

In the current numerical simulation, several assumptions are made to simplify the model:

- (1) The liquid is Newtonian fluid and incompressible;
- (2) Ignoring the super-cooling and volume expansion of water during the solidification process;
- (3) Heat loss through the outer wall of the ISCD is ignored;
- (4) The air flowing in the heat exchange tube is dry air;
- (5) The ice side is laminar, and the influence of buoyancy can be ignored.

The air in the heat exchange tube is a non-isothermal movement, and the temperature changes significantly during the heat exchange process, and the density change caused by temperature cannot be ignored. In this case, the Boussinesq approximation of air density can be taken: the viscous dissipation of air is negligible. In addition to density, other physical property parameters are constants. The Navier-Stokes equation after the Boussinesq approximation is<sup>[38]</sup>:

$$\frac{\partial u_i}{\partial \tau} + u_j \frac{\partial u_i}{\partial x_j} = -\frac{1}{\rho} \frac{\partial p}{\partial x_i} + \frac{\partial}{\partial x_j} \left[ \mu \left( \frac{\partial u_i}{\partial x_j} + \frac{\partial u_j}{\partial x_i} \right) \right] + g\beta\Delta T\delta_{zi} \quad (1)$$

1 where,  $\mu$  is the dynamic viscosity coefficient ( $\text{N}\cdot\text{s}/\text{m}^2$ ),  $\beta$  is the coefficient of volume expansion,  
 2  $\delta_{zi}$  is the Kronecker operator, and  $g$  is the acceleration due to gravity ( $\text{m}/\text{s}^2$ ).

3 The governing equations for the model are the conservation equations for mass, momentum,  
 4 and energy as follows:

5 Equation for conservation of mass<sup>[39]</sup>:

$$6 \quad -\frac{\partial \rho}{\partial \tau} = \nabla \cdot (\rho \vec{V}) \quad (2)$$

7 where,  $\vec{V}$  is the velocity vector ( $\text{m}/\text{s}$ ) and  $\tau$  is the time ( $\text{s}$ ).

8 Equation for conservation of momentum<sup>[40]</sup>:

$$9 \quad \rho \frac{\partial \vec{U}}{\partial \tau} + \rho (\vec{V} \cdot \nabla) \vec{V} = -\nabla p + \mu \cdot \nabla^2 \vec{V} + \rho \alpha (T - T_r) \vec{g} + \vec{S} \quad (3)$$

$$10 \quad S = \frac{(1 + \gamma)^2}{(\gamma^3 + \omega)} C_m \vec{V} \quad (4)$$

11  
 12 where,  $p$  is the pressure ( $\text{Pa}$ ),  $\mu$  is the dynamic viscosity coefficient ( $\text{N}\cdot\text{s}/\text{m}^2$ ),  $\alpha$  is the  
 13 coefficient of thermal expansion ( $1/\text{K}$ ),  $g$  is the acceleration due to gravity ( $\text{m}/\text{s}^2$ ),  $S$  is the source  
 14 term used to account for changes in fluid velocity during solidification ( $\text{m}/\text{s}$ ),  $\gamma$  indicates the liquid  
 15 part,  $Tr$  is the temperature value of the reference surface,  $\omega$  is a small value (0.001) to avoid zero  
 16 division,  $C_m$  is a mushy zone constant usually set to the range of  $1 \times 10^4 - 1 \times 10^7$ , and in the current  
 17 work  $C_m$  is assumed to be a constant, and its value is set to  $1 \times 10^5$ <sup>[26]</sup>.

18 Equation for conservation of energy<sup>[25]</sup>:

$$19 \quad \frac{\partial (h_s + \Delta h)}{\partial \tau} + \nabla \cdot (V \vec{h}_s) = \nabla \cdot \left( \frac{k}{\rho c_p} \nabla h_s \right) \quad (5)$$

20 where,  $h_s$  is the sensible heat enthalpy of the material;  $\Delta h$  is the enthalpy of the phase  
 21 transformation of the material. The values of  $h_s$  and  $\Delta h$  can be calculated from Eqs (6) and (7) <sup>[25]</sup>.

$$22 \quad h_s = h_r + c_p \int_r^T dT \quad (6)$$

$$23 \quad \Delta h = \sum_{i=1}^n \beta_i E \quad (7)$$

$$\gamma = \begin{cases} 0 & T < T_{so} \\ \frac{T - T_{so}}{T_{li} - T_{so}} & T_{so} < T < T_{li} \\ 1 & T > T_{li} \end{cases} \quad (8)$$

where,  $h_r$  is the enthalpy of the reference surface,  $Tr$  is the temperature of the reference surface,  $T_{so}$  is the solidification temperature,  $T_{li}$  is the liquefaction temperature,  $E$  is the enthalpy of the phase transformation of the material in units,  $\gamma$  is the liquid volume fraction can be calculated according to Eq (8).

The  $\kappa$  and  $\varepsilon$  transport equations for the RNG  $\kappa$ - $\varepsilon$  model are as follows<sup>[38]</sup>:

$$\frac{\partial}{\partial \tau}(\rho k) + \frac{\partial}{\partial x_i}(\rho k u_i) = \frac{\partial}{\partial x_j} \left[ \alpha_k \mu_{eff} \frac{\partial k}{\partial x_j} \right] + G_k + G_b - \rho \varepsilon - Y_M + S_k \quad (9)$$

$$\frac{\partial}{\partial \tau}(\rho \varepsilon) + \frac{\partial}{\partial x_i}(\rho \varepsilon u_i) = \frac{\partial}{\partial x_j} \left[ \alpha_\varepsilon \mu_{eff} \frac{\partial \varepsilon}{\partial x_j} \right] + C_{1\varepsilon} \frac{\varepsilon}{k} (G_k + C_{3\varepsilon} G_b) - C_{2\varepsilon} \rho \frac{\varepsilon^2}{k} - R_\varepsilon + S_\varepsilon \quad (10)$$

where,  $G_k$  represents the turbulent energy term generated by the laminar velocity gradient,  $G_b$  is a term of turbulent kinetic energy generated by buoyancy,  $Y_M$  represents the contribution of the turbulent pulsation expansion to the dissipation rate in the entire process in the compressible flow. In the compressible flow,  $C_1$ ,  $C_2$ , and  $C_3$  are constants, and  $S_k$  and  $S_\varepsilon$  are user-defined turbulent kinetic energy terms and turbulent dissipation terms.

## 2.5 Simulation settings

Numerical simulations were carried out using the computational fluid dynamics (CFD) software ANSYS FLUENT. The second-order style formula is used to ensure the numerical accuracy. The relaxation factor remains unchanged at the default value and is calculated as convergent when the residuals of mass, momentum, and energy are less than  $10^{-3}$ ,  $10^{-3}$ , and  $10^{-6}$ . The mesh model with 1648926 mesh number and 0.42 mesh quality was selected for time step verification. The pressure-velocity coupling separation algorithm based on pressure SIMPLE is adopted.

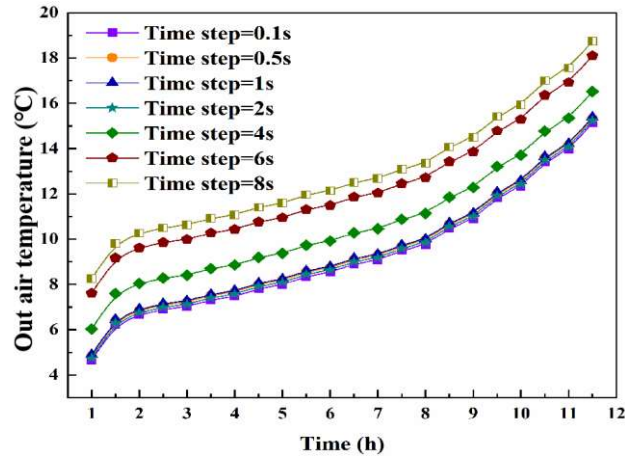


Fig. 5. Time-step validation

As shown in Fig. 5, when the time step size was longer than 2 s, the OAT oscillation was larger, and then the time step size continued to decrease had little effect on the OAT value. In order to reduce the cost of computational time, the time step is set to 2 s. Table 3 shows the boundary conditions during numerical calculation.

Table 3 Boundary conditions

Boundary condition parameters							
	Inlet temperature	Inlet velocity	Initial temperature	Mass flow	Wall temperature	Hydraulic diameter	Re
Parameter	32 °C	10 m/s	-15 °C	32.83 m <sup>3</sup> /h	0 °C	7.5 mm	1.85×
value							10 <sup>4</sup>

## 2.6 Model validation

In order to verify the model, we compared the numerical results of this work with the results of previous studies. To the best of the authors' knowledge, there are no studies on fin-enhanced heat transfer for the ice storage cooling device applied to the refuge chamber in the mine. Another obtained the results of the temperature change at the outlet of the ISCD during heat exchange<sup>[34]</sup>. Since the numerical simulation parameters in case 10 are the same as the experimental conditions in the references<sup>[34]</sup>, and the numerical simulation calculation model in this study is the same as the calculation model in the references<sup>[34]</sup>. Therefore, case 10 was selected for model validation. In order to guarantee the accuracy of the results, the operating conditions, dimensional information, and material properties in the numerical verification are the same as those in the references<sup>[34]</sup>.

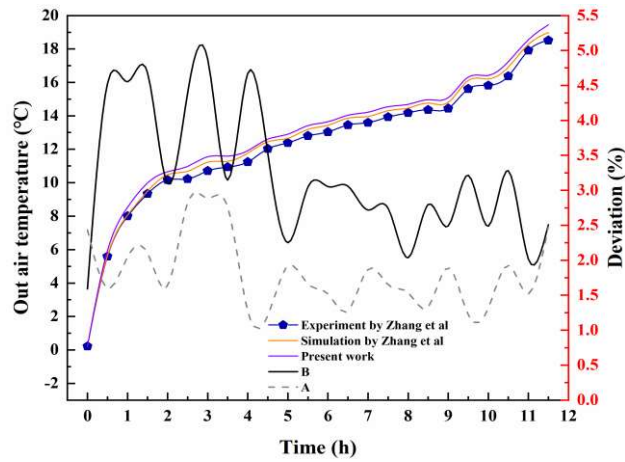


Fig. 6. Model validation

As shown in Fig. 6, A is the error between the numerical results of this study and the numerical results studied by Zhang et al.<sup>[34]</sup>, while B is the error between the numerical results of this study and the experimental results of Zhang et al.<sup>[34]</sup>. Although the current numerical results deviate from the experimental results of Zhang et al.<sup>[34]</sup>, the evolution trend of the overall temperature is exactly the same. Through quantitative analysis, it is inferred that the difference between the current numerical results and the numerical and experimental results in the literature is 2.89% and 4.87%, respectively. Considering the inevitable measurement errors, the difference of the results between this paper and Zhang et al. is acceptable. Therefore, the proposed mathematical model is reliable enough for the following study.

### 3. Results

#### 3.1 Enhance heat transfer characteristics

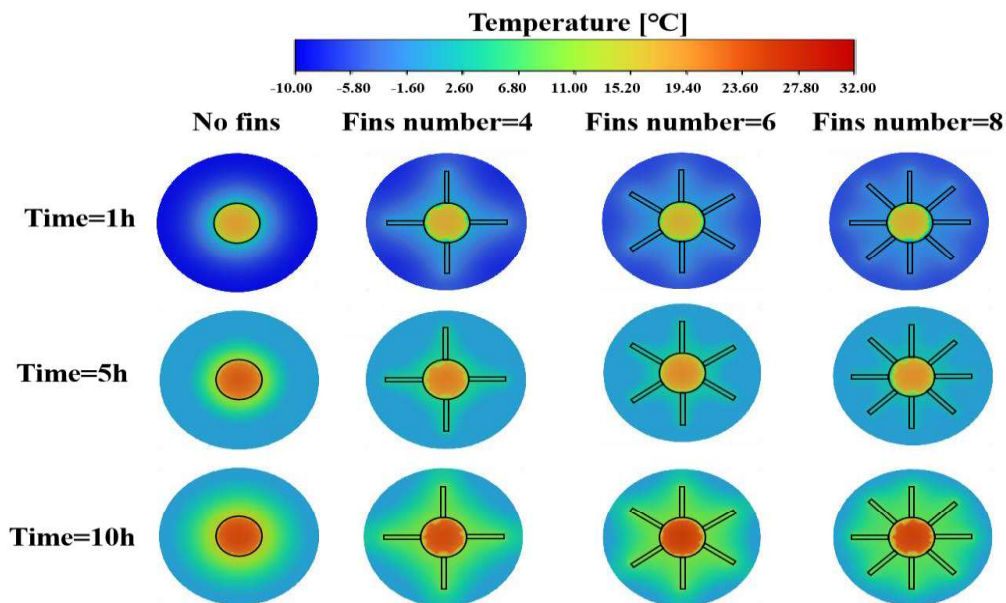
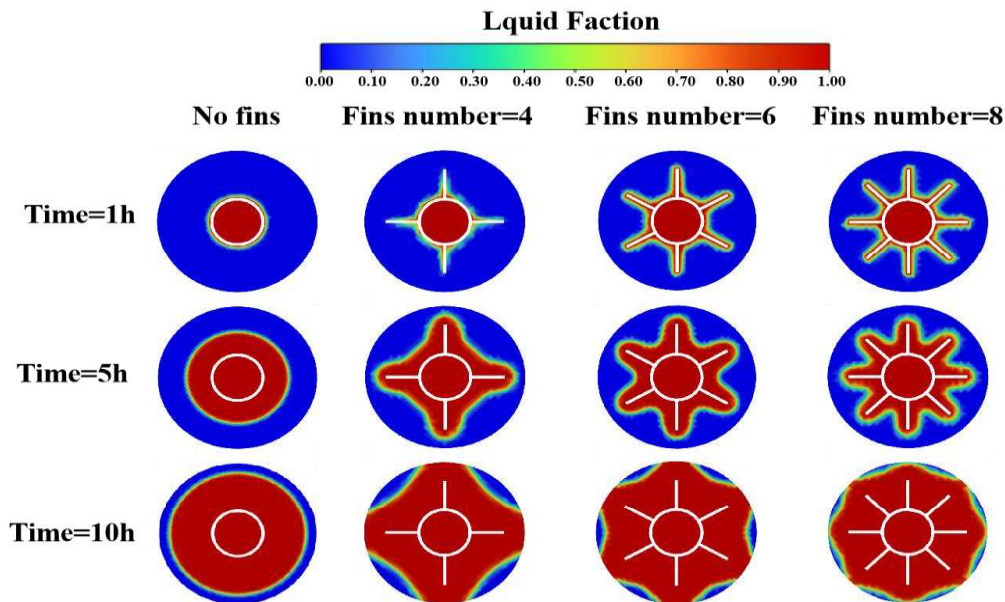


Fig 7. Diagram of temperature distribution with different FNs

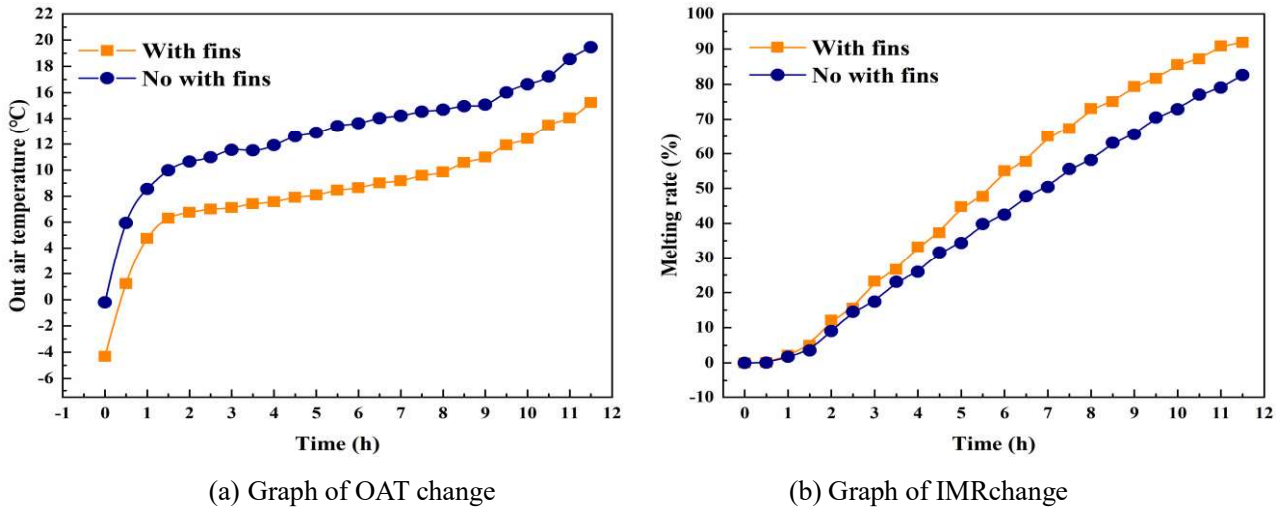
1 Fig. 7 shows the temperature distribution of ISCDs with different fins at 1/2 section and at 1 h,  
 2 5 hrs and 10 hrs. As can be seen from Fig. 7, the temperature in the tube decreases with the increase  
 3 of fins. This can be explained by the fact that increasing the fins is equivalent to increasing the heat  
 4 exchange area, therefore the effect of enhanced heat exchange is achieved, and the OAT decreases.  
 5 After 1 hour of heat exchange, the temperature in the tube of the ISCD with the FN of 0, 4, 6 and 8  
 6 was 8.5 °C, 5.9 °C, 5.2 °C and 4.7 °C, respectively. After 10 hrs, the temperature in the tube of the  
 7 ISCD with the FN of 0, 4, 6 and 8 was 16.4 °C, 13.9 °C, 13.2 °C and 12.4 °C, respectively. It can be  
 8 concluded that adding fins to the ISCD can enhance the heat exchange effect of the ISCD, and the  
 9 heat exchange effect of the ISCD is the best when the FN reaches 8. Considering that the volume  
 10 space of the ISCD is limited, increasing the FN will lead to the reduction of the ice storage capacity,  
 11 which will affect the effective refrigeration time of the whole device.



12 Fig.8. Contour of liquid fraction distribution with different FNs

13 In order to understand the melting behavior in detail, Fig. 8 shows the distribution of melt  
 14 liquid fraction at 1/2 section and at 1 h, 5 hrs, and 10 hrs for ISCDs with different FNs, Obviously,  
 15 the IMR of the ISCD without fins is the slowest, and the insertion of the fins effectively increases  
 16 the IMR. When the duration is 10 hs, for an ISCD without fins, the top ice does not begin to melt,  
 17 while for an ISCD with rectangular fins, the upper ice basically melts. When the FN is 8, the heat  
 18 exchange area is increased, and the heat transfer between the fins and the ice is strengthened. As a  
 19 result, the ice melts faster with a device with 8 fins. It can be seen from Fig. 9 that with the increase  
 20 of the FN, the IMR in the device also increases, and after 10 hrs, the ice in the tube of the ISCD  
 21 with the FN 0, 4, 6 and 8 melts by 72.8%, 79.2%, 84.2% and 85.5%, respectively. It can be  
 22

1 concluded that the ISCD with the addition of fins increases the IMR.



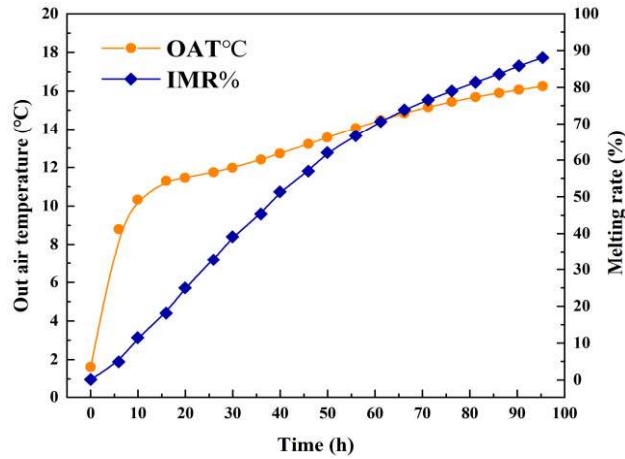
2  
3  
4 Fig. 9. Enhanced heat transfer performance curve

5 Fig. 9 shows a comparison of the heat transfer performance of an ISCD without fins and an  
6 ISCD with 8 fins, the FH is 20 mm and the FT is 2 mm. As can be seen from Fig. 9 (a), the addition  
7 of fins can enhance the heat transfer effect of the ISCD. When there are no fins, the OAT of the  
8 ISCD after 11 hrs of heat exchange is 19.5 °C, and the average outlet temperature (AOT) during heat  
9 exchange is 12.9 °C. After adding fins, the OAT of the ISCD after 11 hrs of heat exchange was  
10 15.2 °C, and the AOT during heat exchange was 8.5 °C, and the average heat exchange efficiency  
11 was increased by 34.12%. In the whole heat exchange process, the temperature change of the outlet  
12 of the single-tube drum ISCD can be divided into three stages. The first stage is 0-2 hrs, due to the  
13 influence of the temperature increase of ice, the air and ice are sensible heat exchange, the OAT  
14 rises rapidly. The second stage is 2-9 hrs, the ice begins to melt and release the latent heat, and this  
15 stage releases much cold energy, thus the OAT rises relatively gradually. The third stage is 9 hrs  
16 later, and the stage is basically melted, which is mainly based on sensible heat exchange caused by  
17 the rise of water temperature, and the cold energy released by the rise of water temperature is less,  
18 resulting in a faster rise in OAT. It can be seen from Fig. 9 (b) that the ice melting rate (IMR) of the  
19 ISCD is increased after the addition of fins, and the IMR of the ISCD is 82.5% after 11 hrs of heat  
20 exchange without fins, and the IMR of the ISCD is 91.8% after the addition of fins. It can be  
21 concluded that after 11 hrs of heat exchange, the OAT of the ISCD was reduced by 4.3°C, and the  
22 IMR was increased by 9.3%.

### 23 3.2 Heat Transfer Performance Analysis of 96 hrs

24 Current studies have shown that the indoor temperature of the MRC should be lower than

1 35 °C during the 96 hr evacuation period. Therefore, the optimised ISCD needs to meet the cooling  
 2 requirements of the MRC. In order to reflect the cooling characteristics of the optimised ISCD  
 3 within 96 hrs, a numerical model of the ISCD with 8 fins, FT is 2 mm, FH is 50 mm and 100 mm  
 4 heat-affected radius of heat exchanger tube was selected for the current study.

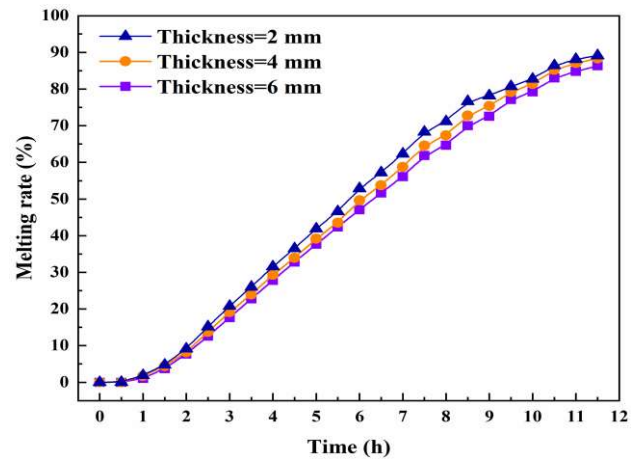
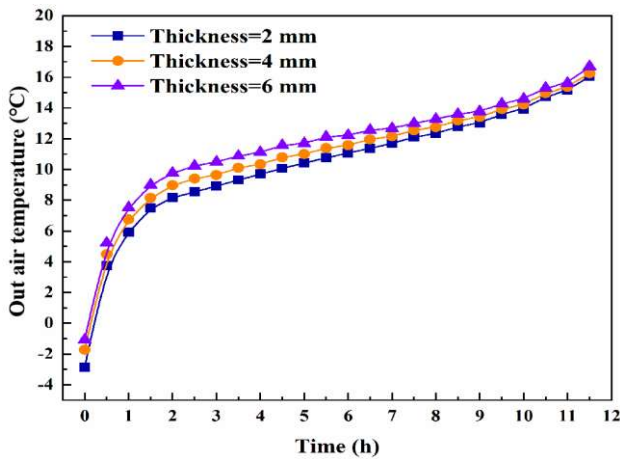


5  
6 Fig. 10. Heat transfer performance curve for 96 hours

7 As shown in Fig. 10, the cooling characteristics of the optimised ISCD within 96 hrs are  
 8 reflected, and it can be seen from the figure that the IMR at the OAT increases with the increase of  
 9 heat exchange time. The OAT of the ISCD increased significantly in the first 15 hrs, while the OAT  
 10 of the ISCD reached 11.3 °C after 15 hrs of heat exchange, and the IMR only reached 15%, which  
 11 indicated that the ISCD was mainly based on sensible heat exchange between air and ice in the first  
 12 15 hrs. From 15 hrs to 55 hrs, the temperature rise at the outlet of ISCD is small, and the ice melts  
 13 by 70%, since the melting of the ice during this time releases a large amount of latent heat of phase  
 14 change, absorbs a lot of heat from the air, and the OAT is maintained between 11-14 °C. During the  
 15 period of 55-96 hrs, the ice storage capacity has melted by more than 70%, and the OAT slowly  
 16 rises from 14 °C to 16.25 °C. Since the specific heat capacity of the water is large and can absorb  
 17 more heat, and this stage mainly relies on the increase of the water temperature to absorb the heat of  
 18 the air in order to achieve the required cooling. It can be concluded that when the IAT is 32 °C and  
 19 the IAV is 10 m/s, the OAT is within 16.5 °C after 96 hr of heat exchange, which can meet the  
 20 cooling requirements of the refuge chamber for 96 hrs.

### 21 3.3 Sensitivity analysis

#### 22 3.3.1 Effect of the FT



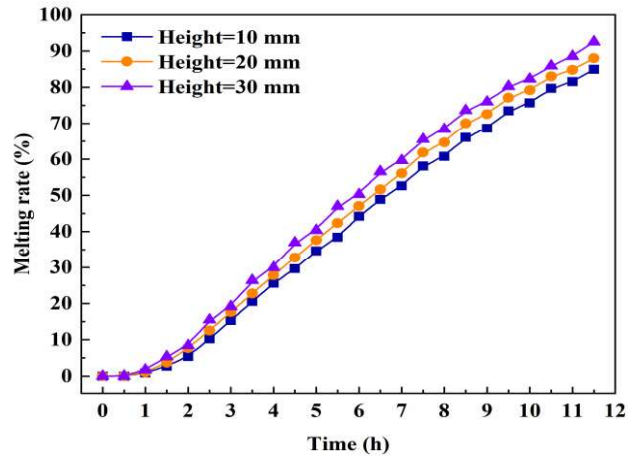
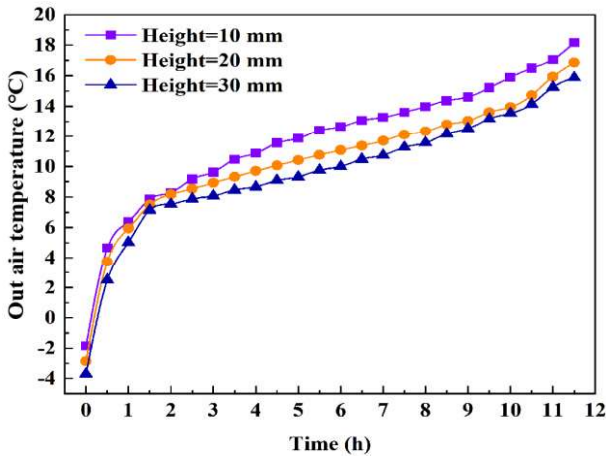
(a) Effect of FT on OAT

(b) Effect of fin FT on IMR

Fig.11. Influence curves of different fin FTs on heat transfer performance

Fig. 11 shows the relationship between different FT and the OAT of the ISCD and the IMR when the IAT is 32 °C, the IAV is 10 m/s, the FN is 4, and the FH is 20 mm. From Fig. 11 (a), it can be concluded that the OAT of the ISCD increases with the increase of FT, which indicates that the larger the FT, the worse the cooling effect of the ISCD. This is because the FT, the higher the thermal resistance, could result in less effective heat transfer. The OAT of the ISCD increases with time, and the overall trend can be divided into three stages. The first stage is when the temperature of the ice rises to absorb the heat in the air, the second stage is when the ice melts and absorbs the heat in the air, and the third stage is when the water temperature rises after the ice melts and absorbs the heat in the air. After 11 hr of heat exchange, the FT is 2 mm, 4 mm and 6 mm, and the corresponding OATs are 16.06 °C, 16.26 °C and 16.69 °C, respectively. The cooling temperature difference after 11 hrs is between 15-16 °C. As can be seen from Fig. 11(b), the smaller the FT, the higher the IMR of ISCD. After 11 hr of heat exchange, the FT increased from 2 mm to 6 mm, the IMR decreased from 89.12% to 86.30%, and the IMR decreased by 2.9%. With the FT, the smaller the heat passing through the fin, and the smaller the heat transfer can be obtained by the calculation formula of heat conduction.

### 3.3.2 Effect of the FH



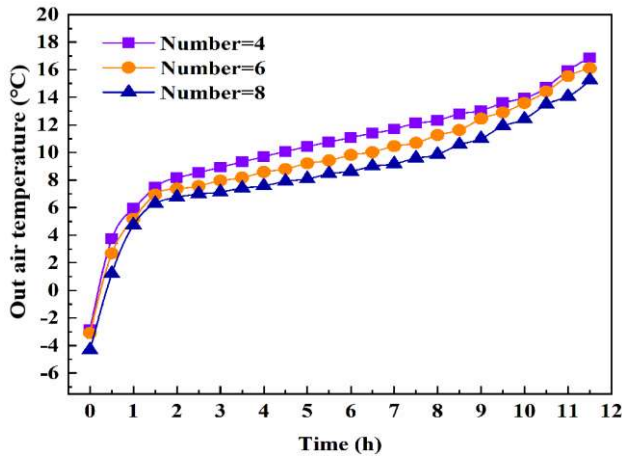
(a) Effect of FH on OAT

(b) Effect of FH on IMR

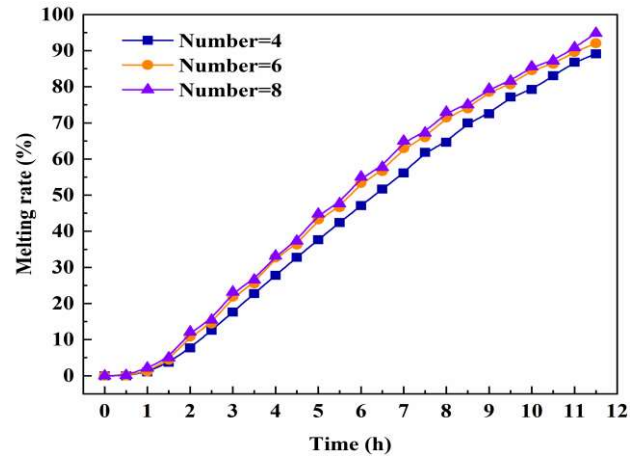
Fig. 12. Influence curves of different FHs on heat transfer performance

Fig. 12 plots the effects of different FHs on the OAT and IMR at an IAT of 32 °C, an IAV of 10 m/s, the FNs is 4, and a FT of 2 mm. As shown in Fig. 12(a), it can be concluded that different FHs affect the cooling effect of the ISCD, and the OAT of the ISCD decreases with the increase of the FH, which indicates that the larger the FH, the better the cooling effect of the ISCD. The whole process can be divided into three stages, the first stage is the exchange of sensible heat between air and ice, the heat exchange time is short, and the temperature rise is large. The second stage is the exchange of latent heat between air and ice, and the heat exchange time of the second stage decreases with the increase of FH, and the temperature rises slowly. The third stage is the sensible heat exchange between air and water. The increase in the FH will increase the heat exchange area between the fins and the ice, and the effect of enhanced heat exchange will be achieved. When the FH is 10 mm, 20 mm and 30 mm, the OAT after 11hr heat exchange is 18.18 °C, 16.06 °C and 15.88 °C, respectively, and the temperature difference between the inlet and outlet after 11hr cooling is between 13-16 °C. As shown in Fig. 12(b), the higher the FH, the larger the IMR, and the ice in the ISCD melted by 84.94%, 89.12% and 92.54% respectively after 11 hr of heat exchange. Overall, it can be seen that increasing the FH can improve the ice utilisation efficiency and optimise the cooling effect of the ISCD.

### 3.3.3 Effect of the FN



(a) Effect of FN on OAT



(b) Effect of FN on IMR

Fig. 13. Influence curves of different FNs on heat transfer performance

Fig. 13 plots the effects of different FNs on the OAT and IMR at an IAT of 32 °C, an IAV of 10 m/s, a FH of 20 mm, and a FT of 2 mm. Fig. 13(a) shows the effect of changing the FN on the outlet air temperature, and it can be seen that the outlet air temperature is proportional to the test time, which increases with time, and the outlet air temperature gradually decreases with the increase of the FN. This is because the increase in the FN in the heat transfer process of the ISCD will increase the heat transfer area, which will absorb more heat in the air, thus the outlet air temperature will be lower. When the FN is 4, 6 and 8, the air temperature at the outlet of the ISCD is 16.06 °C, 15.22 °C and 14.23 °C after 11 hr of heat exchange, and the average OAT is 10.40 °C, 9.48 °C and 8.46 °C during the 11 hr heat exchange cycle, and the cooling efficiency is 47.32%, 49.65% and 52.39% respectively. It can be seen from Fig. 13(b) that the higher the FN, the larger the IMR, the ice melted 89.12%, 92.08% and 94.84% respectively after 11 hr heat exchange, and the advantage of increasing the FN is that the heat transfer area can be greatly increased, and the thermal conductivity efficiency of the ice storage side is enhanced, However, an increase in the FN will take up most of the space and reduce the amount of ice stored. Therefore, the FN needs to be controlled within a certain range, and the ice storage capacity of more than 83.33% needs to be maintained while improving the heat exchange efficiency<sup>[33]</sup>.

## 4. Discussion

### 4.1 Application analysis after optimization of ISCD

After the ISCD was optimised by adding fins, the influence of the FT, FH and FN on the ISCD was analyzed by numerical simulation. According to the principle of heat transfer, it can be concluded that increasing FT under the condition that the heat transfer temperature difference is

1 unchanged will lead to the decrease of heat transfer coefficient, and increasing the FN and the FH  
 2 can increase the heat transfer area and thus enhance the heat transfer. However, while increasing the  
 3 FN and the FH, it is necessary to take into account the ice storage capacity of the ISCD, and the ice  
 4 storage capacity should be more than 83.33%<sup>[34]</sup>. The ice storage capacity of the ISCD can be  
 5 calculated according to the following formula:

$$Q = \frac{\frac{\pi \times (R_0^2 - R_2^2)}{4} - H \times T \times N}{\frac{\pi \times R_0^2}{4}} \times 100 \% \quad (11)$$

7 where  $R_0$  is the diameter of the ice bucket,  $R_2$  is the outer diameter of the heat exchanger tube,  
 8  $H$  is the FH,  $T$  is the FT,  $N$  is the FNs, and the length of the fins is the same as the length of the ice  
 9 bucket. After numerical simulation analysis, the optimal FH is 30 mm, the FT is 2 mm, and the FN  
 10 is 8. The total volume of the ISCD minus the volume occupied by the fins and thermofluid pipes is  
 11 the ice storage volume. The ratio of the volume of ice storage to the total volume of the ISCD is the  
 12 ice storage capacity. The ice storage capacity of the ISCD under the optimal fin size can be obtained  
 13 by Eq.11 which is 84.88%, this can meet the ice storage requirements of the ISCD. However, if the  
 14 FN continues to increase, the ice storage capacity of the ISCD will be lower than 83.33%, in the  
 15 case, the FN is larger than 8, the effective refrigeration time of the ISCD will decrease.

16 The ISCD has been optimised to improve the cooling performance, which can improve its  
 17 operation efficiency in practical applications, such as saving energy, reducing transportation costs,  
 18 and improving the scope of application. For the temperature control requirements of the  
 19 underground MRC, the corresponding supply air temperature (SAT) needs to be reached at different  
 20 initial surrounding rock temperatures to meet the cooling requirements of the MRC for 96 hrs<sup>[41]</sup>.  
 21 When the temperature of the surrounding rock is greater than 27 °C, the compressed air cooling of  
 22 the mine will not be able to meet the temperature control demand, and the compressed air needs to  
 23 be cooled and then sent to the MRC to achieve the temperature control demand<sup>[42,43]</sup>. When the  
 24 temperature of the surrounding rock is 30 °C, 31 °C, 32 °C, 33 °C and 34 °C, the SAT of the MRC  
 25 needs to be lower than 23.28 °C, 21.83 °C, 20.38 °C, 18.93 °C and 17.48 °C, respectively to meet the  
 26 cooling demand of the MRC for 96 hrs<sup>[44]</sup>. When the IAT was 30 °C, 31 °C, 32 °C, 33 °C and 34 °C,  
 27 respectively, after 96 rh heat exchange experiment, the OAT was 24.70 °C, 25.70 °C, 25.96 °C, 27.65 °C  
 28 and 28.52 °C, respectively<sup>[34]</sup>. It can be seen that the ISCD cannot meet the air supply requirements

1 of the MRC before optimisation. By increasing the fins, the cooling efficiency of the ISCD can be  
 2 increased by 34.12% when the FT is 2 mm and the FH is 20 mm, and the FN is 8.

3 **Table 4:** Comparison of OATs after 96 hrs

IAT (°C)	OAT without fins <sup>[34]</sup> (°C)	OAT With fins (°C)	SAT (°C) <sup>[44]</sup>
30	24.70	16.27	23.28
31	25.70	16.93	21.83
32	25.96	17.10	20.38
33	27.65	18.22	18.93
34	28.52	17.79	17.48

4 From **Table 4**, it can be concluded that after adding fins, the ISCD can meet the air supply  
 5 requirements of the MRC when the IAT is less than 34 °C. For IAT above 34 °C, the performance of  
 6 the ISCD can be improved by increasing the FH, or multiple ISCDs can be equipped to meet the  
 7 cooling requirements.

## 8 **4.2 Comparison of the performance of different fins**

9 Currently, there is a wide range of research on the performance optimisation of phase change  
 10 energy storage devices, and previous researchers have developed Circular superimposed  
 11 longitudinal fins, triangular fins, bionic palmate blade fins, Spiderweb-like fins, etc. These fin  
 12 shapes greatly improve the melting and solidification characteristics of phase change energy storage  
 13 devices. However, with the diversification and complexity of fin shapes, the storage space of phase  
 14 change materials in phase change energy storage devices is getting smaller and smaller. While  
 15 improving the heat exchange efficiency of the phase change coarse energy device, it is also  
 16 necessary to take into account the storage space of phase change materials. The application of the  
 17 ISCD mentioned in the current work is the underground MRC, and the ice storage volume of the ice  
 18 storage device must meet the temperature control requirements of the MRC. Therefore, in the  
 19 optimisation of the ISCD, it is not possible to unilaterally consider improving the heat exchange  
 20 efficiency, but also to consider the ice storage capacity of the ISCD. And the fins should not occupy  
 21 too much of the volume of the ISCD, and the ice storage volume of the ISCD is suggested to reach  
 22 more than 83.33%.

23 As shown in **Table 5**, the performance of five phase change energy storage devices with  
 24 different fins was compared and analyzed. It can be seen that with the more complex fin shape and

1 the larger the number of fins, the more obvious the heat exchange effect of the phase change energy  
 2 storage device. It is noted that the fins occupy a large amount of space, resulting in smaller and  
 3 smaller effective volume. Although the rectangular fin used in this paper is lower than other fins in  
 4 terms of heat exchange effect, the coarse storage space of the phase change material can be  
 5 guaranteed to be more than 84.88%, which can not only meet the application conditions but also  
 6 improve the heat transfer performance of the ice storage device.

7 [Table 5](#). Comparative analysis of different fins

Fin type	Phase change materials	Number of fins	Effective volume ratio	Heat transfer effect
Circular superimposed longitudinal fins <sup>[45]</sup>	Li <sub>2</sub> CO <sub>3</sub> -K <sub>2</sub> CO <sub>3</sub> -Na <sub>2</sub> CO <sub>3</sub>	4	77.50%	The solidification time of PCM was shortened by 1117 s.
External triangular fins <sup>[40]</sup>	Alumina nanoparticle and Paraffin	8	71.26%	The melting time of PCM was shortened by 1800 s.
Palmate leaf-shaped fins is designed by bionic techniques <sup>[31]</sup>	Lauric acid	6	64.35%	The PCM melting time shortened by 21.0 %.
Spiderweb-like fins <sup>[25]</sup>	Lauric acid	12	60.25%	The solidification time shortened by 47.9 %.
Rectangular fins	Ice	8	84.88%	The melting time of PCM was shortened by 18.8%.

## 8 **5. Conclusion**

9 In this study, according to the temperature control requirements of underground mine refuge  
 10 chambers, the ISCD applied to underground MRC was optimised, and the effects of FH, FT and FN  
 11 on the performance improvement effect of the ISCD were investigated in a systematic manner.  
 12 Compared with the traditional ISCD, the optimised heat transfer device can improve both the heat  
 13 transfer performance and the application range of the ISCD. The main conclusions are summarized  
 14 below:

1 (1) The numerical simulation analysis shows that the FN is the key factor to improve the heat  
2 transfer performance of the ISCD, but too many fins will lead to too low ice storage capacity of the  
3 ISCD, which will affect the effective cooling time of the ISCD. In the current study, the optimal FN  
4 is 8.

5 (2) Through the simulation results, it is concluded that the increase of the thermal conductivity  
6 and thermal resistance caused by the larger the FT will reduce the heat exchange performance of the  
7 ISCD, while the increase of the FN and the FH can increase the heat exchange area and improve the  
8 heat transfer performance. The ISCD with a FH of 30 mm, a FT of 2 mm, and a FN of 8 is selected  
9 for the best heat transfer performance.

10 (3) When the FN increased from 4 to 8, the average OAT of the ISCD was 10.4 °C and 8.46 °C  
11 respectively after the 11 hr heat exchange cycle, and the IMR increased by 5.72%.

12 (4) Compared with the ISCD without fins, the cooling efficiency of the ISCD increased by  
13 34.12% and the IMR increased by 9.3% after the addition of fins.

14 (5) When the number of fins is 8, the ice storage capacity of the ice storage device is more than  
15 84.88%, and the melting time is of ice shortened by 2.5 hrs (a reduction of 18.8%) compared with  
16 the ISCD without fins.

17 (6) The OAT of the optimised ISCD is within 16.3 °C after 96 hr of heat exchange, which can  
18 meet the temperature control requirements of the MRC within 96 hrs.

19

## 20 **Credit authorship contribution statement**

21 Weishuang Guo: Investigation, Writing – original draft. Zujing Zhang: Conceptualization,  
22 Project administration. Xing Liang: Discussion, Writing – review & editing. Hongwei Wu:  
23 Writing – review & editing. Liang Ge: Formal analysis. Ruiyong Mao: Methodology.

## 24 **Declaration of competing interest**

25 The authors declare that they have no known competing financial interests or personal  
26 relationships that could have appeared to influence the work reported in this paper.

## 27 **Acknowledgments**

28 The authors would like to thank the financial support from the National Natural Science  
29 Foundation of China ([52168013](#)), the Natural Science Foundation of Guizhou Province

1 (ZK[2022]151) and the State Key Laboratory of Gas Disaster Detecting, Preventing and Emergency  
2 Controlling Open-fund Project (2021SKLKF10).

3

## 4 **References**

- 5 [1] P. Yang, S. Peng, N. Benani, L. Dong, X. Li, R. Liu, G. Mao, An integrated evaluation on  
6 china's provincial carbon peak and carbon neutrality, *J. Clean Prod.* 377 (2022) 134497,  
7 <https://doi.org/https://doi.org/10.1016/j.jclepro.2022.134497>.
- 8 [2] Y. Wei, K. Chen, J. Kang, W. Chen, X. Wang, X. Zhang, Policy and management of carbon  
9 peaking and carbon neutrality: a literature review, *Engineering* 14 (2022) 52-63,  
10 <https://doi.org/https://doi.org/10.1016/j.eng.2021.12.018>.
- 11 [3] R. Li, Q. Liu, W. Cai, Y. Liu, Y. Yu, Y. Zhang, Echelon peaking path of china's provincial  
12 building carbon emissions: considering peak and time constraints, *Energy* 271 (2023) 127003,  
13 <https://doi.org/https://doi.org/10.1016/j.energy.2023.127003>.
- 14 [4] L. Rovira-Alsina, M.D. Balaguer, S. Puig, Thermophilic bio-electro carbon dioxide  
15 recycling harnessing renewable energy surplus, *Bioresour. Technol.* 321 (2021) 124423,  
16 <https://doi.org/https://doi.org/10.1016/j.biortech.2020.124423>.
- 17 [5] J.D. Osorio, M. Panwar, A. Rivera-Alvarez, C. Chrysostomidis, R. Hovsopian, M.  
18 Mohanpurkar, S. Chanda, H. Williams, Enabling thermal efficiency improvement and waste heat  
19 recovery using liquid air harnessed from offshore renewable energy sources, *Appl. Energy* 275  
20 (2020) 115351, <https://doi.org/https://doi.org/10.1016/j.apenergy.2020.115351>.
- 21 [6] V.J. A., K.A.B. T., Ocean and geothermal energy systems, *Proc. Ieee* 105 (11) (2017)  
22 2147-2165, <https://doi.org/10.1109/JPROC.2017.2699558>.
- 23 [7] A. Dupré, P. Drobinski, B. Alonzo, J. Badosa, C. Briard, R. Plougonven, Sub-hourly  
24 forecasting of wind speed and wind energy, *Renew. Energy* 145 (2020) 2373-2379,  
25 <https://doi.org/https://doi.org/10.1016/j.renene.2019.07.161>.
- 26 [8] M.K.H. Rabaia, M.A. Abdelkareem, E.T. Sayed, K. Elsaid, K. Chae, T. Wilberforce, A.G.  
27 Olabi, Environmental impacts of solar energy systems: a review, *Sci. Total Environ.* 754 (2021)  
28 141989, <https://doi.org/https://doi.org/10.1016/j.scitotenv.2020.141989>.
- 29 [9] N. Guillou, G. Chapalain, S.P. Neill, The influence of waves on the tidal kinetic energy  
30 resource at a tidal stream energy site, *Appl. Energy* 180 (2016) 402-415,  
31 <https://doi.org/https://doi.org/10.1016/j.apenergy.2016.07.070>.
- 32 [10] R. Amal, H. Zhao, D. Wang, L. Wang, Renewable energy conversion and storage, *Adv.*  
33 *Energy Mater.* 7 (23) (2017) 1703091, <https://doi.org/https://doi.org/10.1002/aenm.201703091>.
- 34 [11] S. Li, Z. Liu, X. Wang, A comprehensive review on positive cold energy storage  
35 technologies and applications in air conditioning with phase change materials, *Appl. Energy* 255  
36 (2019) 113667, <https://doi.org/https://doi.org/10.1016/j.apenergy.2019.113667>.
- 37 [12] J.L. Espinoza-Acosta, P.I. Torres-Chávez, J.L. Olmedo-Martínez, A. Vega-Rios, S.  
38 Flores-Gallardo, E.A. Zaragoza-Contreras, Lignin in storage and renewable energy applications: a  
39 review, *J. Energy Chem.* 27 (5) (2018) 1422-1438,

- 1 <https://doi.org/https://doi.org/10.1016/j.jechem.2018.02.015>.
- 2 [13] H. Jouhara, L. Montorsi, M.A. Sayegh, Advances and applications of renewable energy,  
3 *Renew. Energy* 165 (2021) 75-76, <https://doi.org/https://doi.org/10.1016/j.renene.2020.11.092>.
- 4 [14] A. Zakaria, F.B. Ismail, M.S.H. Lipu, M.A. Hannan, Uncertainty models for stochastic  
5 optimization in renewable energy applications, *Renew. Energy* 145 (2020) 1543-1571,  
6 <https://doi.org/https://doi.org/10.1016/j.renene.2019.07.081>.
- 7 [15] M. Esen, Thermal performance of a solar-aided latent heat store used for space heating by  
8 heat pump, *Sol. Energy* 69 (1) (2000) 15-25,  
9 [https://doi.org/https://doi.org/10.1016/S0038-092X\(00\)00015-3](https://doi.org/https://doi.org/10.1016/S0038-092X(00)00015-3).
- 10 [16] D. Guo, X. Zhou, Y. Xu, Z. Yin, W. Suo, T. Qin, H. Chen, Structure optimization and  
11 operation characteristics of metal gas storage device based on compressed air energy storage system,  
12 *J. Energy Storage* 72 (2023) 108260, <https://doi.org/https://doi.org/10.1016/j.est.2023.108260>.
- 13 [17] C. Li, Q. Li, R. Ge, Enhancement of melting performance in a shell and tube thermal energy  
14 storage device under different structures and materials, *Appl. Therm. Eng.* 214 (2022) 118701,  
15 <https://doi.org/https://doi.org/10.1016/j.applthermaleng.2022.118701>.
- 16 [18] Q. Ying, H. Wang, Y. Diao, H. Xiang, Metal foam reinforced phase change material energy  
17 storage device: a collaborative optimization strategy for porosity and container shape, *Appl. Therm.*  
18 *Eng.* 235 (2023) 121369, <https://doi.org/https://doi.org/10.1016/j.applthermaleng.2023.121369>.
- 19 [19] C. Chen, Y. Diao, Y. Zhao, Z. Wang, Y. Han, Z. Wang, Y. Liu, D. Fang, T. Zhu, Thermal  
20 performance of cold thermal energy storage system with fin and fin-foam structures, *Appl. Therm.*  
21 *Eng.* 228 (2023) 120459, <https://doi.org/https://doi.org/10.1016/j.applthermaleng.2023.120459>.
- 22 [20] M. Esen, A. Durmuş, A. Durmuş, Geometric design of solar-aided latent heat store  
23 depending on various parameters and phase change materials, *Sol. Energy* 62 (1) (1998) 19-28,  
24 [https://doi.org/https://doi.org/10.1016/S0038-092X\(97\)00104-7](https://doi.org/https://doi.org/10.1016/S0038-092X(97)00104-7).
- 25 [21] M. Ghalambaz, A.A. Melaibari, A.J. Chamkha, O. Younis, M. Sheremet, Phase change heat  
26 transfer and energy storage in a wavy-tube thermal storage unit filled with a nano-enhanced phase  
27 change material and metal foams, *J. Energy Storage* 54 (2022) 105277,  
28 <https://doi.org/https://doi.org/10.1016/j.est.2022.105277>.
- 29 [22] W. Cui, T. Si, X. Li, X. Li, L. Lu, T. Ma, Q. Wang, Heat transfer enhancement of phase  
30 change materials embedded with metal foam for thermal energy storage: a review, *Renewable and*  
31 *Sustainable Energy Reviews* 169 (2022) 112912,  
32 <https://doi.org/https://doi.org/10.1016/j.rser.2022.112912>.
- 33 [23] M. Esen, T. Ayhan, Development of a model compatible with solar assisted cylindrical  
34 energy storage tank and variation of stored energy with time for different phase change materials,  
35 *Energy Conv. Manag.* 37 (12) (1996) 1775-1785,  
36 [https://doi.org/https://doi.org/10.1016/0196-8904\(96\)00035-0](https://doi.org/https://doi.org/10.1016/0196-8904(96)00035-0).
- 37 [24] M. Sheikholeslami, S. Lohrasbi, D.D. Ganji, Numerical analysis of discharging process  
38 acceleration in lhtess by immersing innovative fin configuration using finite element method, *Appl.*  
39 *Therm. Eng.* 107 (2016) 154-166,  
40 <https://doi.org/https://doi.org/10.1016/j.applthermaleng.2016.06.158>.

- 1 [25] L. Wu, X. Zhang, X. Liu, Numerical analysis and improvement of the thermal performance  
2 in a latent heat thermal energy storage device with spiderweb-like fins, *J. Energy Storage* 32 (2020)  
3 101768, <https://doi.org/https://doi.org/10.1016/j.est.2020.101768>.
- 4 [26] Y. Lee, L. Chien, F. Cheung, A. Yang, Numerical and experimental investigations on melting  
5 heat transfer performance of pcm in finned cold thermal energy storage, *Int. J. Heat Mass Transf.*  
6 210 (2023) 124199, <https://doi.org/https://doi.org/10.1016/j.ijheatmasstransfer.2023.124199>.
- 7 [27] X. Liu, X. Qin, Y. Tian, Q. Luo, H. Yao, J. Wang, C. Dang, Q. Xu, S. Lv, Y. Xuan,  
8 Biomimetic optimized vertically aligned annular fins for fast latent heat thermal energy storage,  
9 *Appl. Energy* 347 (2023) 121435, <https://doi.org/https://doi.org/10.1016/j.apenergy.2023.121435>.
- 10 [28] S. Lu, X. Zhai, J. Gao, R. Wang, Performance optimization and experimental analysis of a  
11 novel low-temperature latent heat thermal energy storage device, *Energy* 239 (2022) 122496,  
12 <https://doi.org/https://doi.org/10.1016/j.energy.2021.122496>.
- 13 [29] J.C. Kurnia, A.P. Sasmito, Numerical investigation of heat transfer performance of a rotating  
14 latent heat thermal energy storage, *Appl. Energy* 227 (2018) 542-554,  
15 <https://doi.org/https://doi.org/10.1016/j.apenergy.2017.08.087>.
- 16 [30] C. Zhang, J. Li, Y. Chen, Improving the energy discharging performance of a latent heat  
17 storage (lhs) unit using fractal-tree-shaped fins, *Appl. Energy* 259 (2020) 114102,  
18 <https://doi.org/https://doi.org/10.1016/j.apenergy.2019.114102>.
- 19 [31] Y. Huang, Z. Deng, Y. Chen, C. Zhang, Performance investigation of a biomimetic latent  
20 heat thermal energy storage device for waste heat recovery in data centers, *Appl. Energy* 335 (2023)  
21 120745, <https://doi.org/https://doi.org/10.1016/j.apenergy.2023.120745>.
- 22 [32] S. Wang, L. Jin, Z. Han, Y. Li, S. Ou, N. Gao, Z. Huang, Discharging performance of a  
23 forced-circulation ice thermal storage system for a permanent refuge chamber in an underground  
24 mine, *Appl. Therm. Eng.* 110 (2017) 703-709,  
25 <https://doi.org/https://doi.org/10.1016/j.applthermaleng.2016.08.192>.
- 26 [33] Y. Du, W. Gai, L. Jin, W. Sheng, Thermal comfort model analysis and optimization  
27 performance evaluation of a multifunctional ice storage air conditioning system in a confined mine  
28 refuge chamber, *Energy* 141 (2017) 964-974,  
29 <https://doi.org/https://doi.org/10.1016/j.energy.2017.09.123>.
- 30 [34] Z. Zhang, W. Guo, H. Wu, L. Ge, Xing Liang, R. Mao, Thermal performance of an ice  
31 storage device for cooling compressed mine air in high-temperature mine refuge chambers, *Appl.*  
32 *Therm. Eng.* 233 (2023) 121101,  
33 <https://doi.org/https://doi.org/10.1016/j.applthermaleng.2023.121101>.
- 34 [35] W. Guo, Z. Zhang, H. Wu, L. Ge, X. Liang, R. Mao, Experimental study on cooling and  
35 dehumidification performance of an ice storage air conditioner used in underground refuge chamber,  
36 *Int. Commun. Heat Mass Transf.* 146 (2023) 106930,  
37 <https://doi.org/https://doi.org/10.1016/j.icheatmasstransfer.2023.106930>.
- 38 [36] A. Kumar, S.K. Saha, Performance study of a novel funnel shaped shell and tube latent heat  
39 thermal energy storage system, *Renew. Energy* 165 (2021) 731-747,  
40 <https://doi.org/https://doi.org/10.1016/j.renene.2020.11.023>.

- 1 [37] D. Yang, R. Shi, H. Wei, J. Du, J. Wang, Investigation of the performance of a cylindrical  
2 pcm-to-air heat exchanger (pahe) for free ventilation cooling in fluctuating ambient environments,  
3 *Sust. Cities Soc.* 51 (2019) 101764, [https://doi.org/https://doi.org/10.1016/j.scs.2019.101764](https://doi.org/10.1016/j.scs.2019.101764).
- 4 [38] H. Wang, Numerical calculation methods and applications of hvac fluid flow, Science Press,  
5 Beijing, 2013.
- 6 [39] A. Sharma, P. Parth, S. Shobhana, M. Bobin, B.K. Hardik, Numerical study of ice freezing  
7 process on fin aided thermal energy storage system, *Int. Commun. Heat Mass Transf.* 130 (2022)  
8 105792, [https://doi.org/https://doi.org/10.1016/j.icheatmasstransfer.2021.105792](https://doi.org/10.1016/j.icheatmasstransfer.2021.105792).
- 9 [40] A.M. Abdulateef, J. Abdulateef, K. Sopian, S. Mat, A. Ibrahim, Optimal fin parameters used  
10 for enhancing the melting and solidification of phase-change material in a heat exchanger unite,  
11 *Case Stud. Therm. Eng.* 14 (2019) 100487,  
12 [https://doi.org/https://doi.org/10.1016/j.csite.2019.100487](https://doi.org/10.1016/j.csite.2019.100487).
- 13 [41] Z. Zhang, H. Wu, K. Wang, R. Day, Y. Yuan, Air quality control in mine refuge chamber with  
14 ventilation through pressure air pipeline, *Process Saf. Environ. Protect.* 135 (2020) 46-58,  
15 [https://doi.org/https://doi.org/10.1016/j.psep.2019.12.014](https://doi.org/10.1016/j.psep.2019.12.014).
- 16 [42] X. Gao, Z. Zhang, Y. Xiao, Modelling and thermo-hygrometric performance study of an  
17 underground chamber with a long vertical earth-air heat exchanger system, *Appl. Therm. Eng.* 180  
18 (2020) 115773, [https://doi.org/https://doi.org/10.1016/j.applthermaleng.2020.115773](https://doi.org/10.1016/j.applthermaleng.2020.115773).
- 19 [43] Z. Zhang, H. Wu, K. Wang, R. Day, Y. Yuan, Thermal performance of a mine refuge chamber  
20 with human body heat sources under ventilation, *Appl. Therm. Eng.* 162 (2019) 114243,  
21 [https://doi.org/https://doi.org/10.1016/j.applthermaleng.2019.114243](https://doi.org/10.1016/j.applthermaleng.2019.114243).
- 22 [44] Z. Zhang, W. Guo, X. Gao, H. Wu, R. Mao, Investigation on temperature control based on  
23 cooled mine compressed air for mine refuge chamber with high-temperature surrounding rock, *Int. J.*  
24 *Therm. Sci.* 187 (2023) 108201, [https://doi.org/https://doi.org/10.1016/j.ijthermalsci.2023.108201](https://doi.org/10.1016/j.ijthermalsci.2023.108201).
- 25 [45] J. Ma, H. Xu, S. Liu, H. Peng, X. Ling, Numerical study on solidification behavior and exergy  
26 analysis of a latent heat storage unit with innovative circular superimposed longitudinal fins, *Int. J.*  
27 *Heat Mass Transf.* 169 (2021) 120949,  
28 [https://doi.org/https://doi.org/10.1016/j.ijheatmasstransfer.2021.120949](https://doi.org/10.1016/j.ijheatmasstransfer.2021.120949).

29

## **Declaration of Interest Statement**

We declare that we have no financial and personal relationships with other people or organizations that can inappropriately influence our work, there is no professional or other personal interest of any nature or kind in any product, service and/or company that could be construed as influencing the position presented in, or the review of, the manuscript entitled '*Numerical study on the heat transfer performance of mine ice-storage cooling device*'.

## **Credit author statement**

**Weishuang Guo:** Investigation, Writing - Original Draft. **Zujing Zhang:** Conceptualization, Project administration. **Xing Liang:** Writing - Review & Editing. **Hongwei Wu:** Writing - Review & Editing. **Liang Ge:** Formal analysis. **Ruiyong Mao:** Methodology.